Available online at www.sciencedirect.com

SciVerse ScienceDirect

Ceramics International 38 (2012) 4209–4216

CERAMICS INTERNATIONAL

www.elsevier.com/locate/ceramint

Preparation and characterization of tin oxide, SnO_2 nanoparticles decorated graphene

H.N. Lim [a,*], R. Nurzulaikha [b], I. Harrison [b], S.S. Lim [b], W.T. Tan [a], M.C. Yeo [a], M.A. Yarmo [c], N.M. Huang [d]

[a] *Department of Chemistry, Faculty of Science, Universiti Putra Malaysia, 43400 UPM Serdang, Selangor, Malaysia*

[b] *School of Chemical and Environmental Engineering, Faculty of Engineering, The University of Nottingham Malaysia Campus, Jalan Broga, 43500 Semenyih, Selangor, Malaysia*

[c] *School of Chemical Sciences and Food Technology, Faculty of Science and Technology, Universiti Kebangsaan Malaysia, 43000 Bandar Baru Bangi, Selangor, Malaysia*

[d] *Low Dimensional Materials Research Centre, Department of Physics, Faculty of Science, University of Malaya, 53400 Kuala Lumpur, Selangor, Malaysia*

Received 9 July 2011; accepted 1 February 2012
Available online 9 February 2012

Abstract

SnO_2 nanoparticles/graphene (SnO_2/GP) nanocomposite was synthesized by a facile microwave method. The X-ray diffraction (XRD) pattern of the nanocomposite corresponded to the diffraction peak typical of graphene and the rutile phase of SnO_2 with tetragonal structure. The field emission scanning electron microscope (FESEM) images revealed that the graphene sheets were dotted with SnO_2 nanoparticles with an average size of 10 nm. The X-ray photoelectron spectroscopy (XPS) analysis indicated that the development of SnO_2/GP resulted from the removal of the oxygenous groups on graphene oxide (GO) by Sn^{2+} ions. The nanocomposite modified glassy carbon electrode (GCE) showed excellent enhancement of electrochemical performance when interacting with mercury(II) ions in potassium chloride supporting electrolyte. The current was increased by more than tenfold, suggesting its potential to be used as a mercury(II) sensor.

Keywords: B. Nanocomposite; Graphene; Microscopy; Microwave; Tin oxide; Voltammetry

1. Introduction

Metal oxide nanomaterial/graphene nanocomposites synthesis is fast becoming a research trend amongst scientists from all over the world. Nanomaterials are defined as materials with at least one dimension having a length of less than 100 nm, which can be categorized into two-dimensional (2-D), one-dimensional (1-D) and zero-dimensional (0-D) nanomaterials. Previously, we have produced 0-D Ni_3Se_2 nanoparticles [1], 1-D PbS nanorods [2], 2-D ZnO nanoplates [3] and magnetic Fe_3O_4/ZnO core/shell nanocrystals [4]. Nanostructured materials of metal oxide offer high surface area, non-toxicity, biocompatibility, ease of fabrication and excellent electrochemical catalytic activity [5].

Tin oxide is an n-type semiconductor with a large band gap of 3.6 eV [6]. SnO_2, in particular, is very stable, has got high carrier density and supports enormous concentration of intrinsic and stoichiometry-violating vacancies, which is correlated to its electrical conductivity [7]. It has a wide range of applications as optoelectronic devices, dye-based solar cells, catalysts, gas sensors, electrochromic devices and electrode materials [6–9]. SnO_2 nanoparticles are widely applied for gas sensing application due to their high mobility of conduction electrons, and good chemical and thermal stability under the operating conditions of sensors [10].

Graphene, a single-atom thick 2-D sheet of sp^2 bonded carbon, is experimentally discovered in 2004 [11]. It is the building block for all graphitic materials such as 0-D fullerenes, 1-D single-walled carbon nanotubes (SWCNTs) and three-dimensional (3-D) graphite. Graphene has attracted substantial interest and imagination of the scientific community arising from its remarkable electronic [11], optical [12], mechanical

* Corresponding author. Tel.: +60 16 330 1609.
E-mail address: janet_limhn@yahoo.com (H.N. Lim).

0272-8842/$36.00
doi:10.1016/j.ceramint.2012.02.004

[13], thermal [14] and electrochemical properties [15]. Graphene offers a unique 2-D environment for electron transport and fast heterogeneous electron transfer at their edges [16], as opposed to SWCNTs uniaxial electron conductivity and heterogeneous electron transfer at their two ends [17]. While graphite is brittle, graphene's flexibility is beneficial for use in adaptable electronic and energy storage devices [18]. Graphene exhibits a surface area of 2630 $m^2\ g^{-1}$, which is ~260 times greater than graphite and twice that of CNTs [19].

With large surface area and the aforementioned unique properties, graphene has been an attractive choice as the matrix for nanocomposites [20]. Functionalization of graphene sheets with various nanoparticles can further enhance the properties of graphene. Heterostructures consisting of nanoparticles distributed on the surface of graphene could potentially display not only the unique properties of nanoparticles [21,22] and those of graphene [11,23,24], but also additional novel functionality and properties due to the interaction between the materials. Many exciting applications can be envisioned for these novel heterostructures, such as in chemical sensors, biosensors, nanoelectronics, photovoltaic cells, hydrogen storage, energy storage and photocatalysts [25].

Many types of metal oxide/graphene nanocomposites have been widely reported including Ag_2O/graphene [26], CuO/graphene [27], Cu_2O/graphene [26], CoO/graphene [28], Co_3O_4/graphene [26], Fe_2O_3/graphene [29], Fe_3O_4/graphene [30], Mn_3O_4/graphene [31], NiO/graphene [32], SnO_2/graphene [33–35], TiO_2/graphene [36,37], and ZnO/graphene [26]. These hybrids were fabricated using various approaches such as gas/liquid interface reaction [30,33], hydrothermal [27,29,32,37], in situ chemical synthesis [35], in situ oxidation route [26], laser irradiation [28], microwave [34], sonochemical [36] and ultrasonication [31].

Mercury is one of the most toxic heavy metals known to organisms and the environment as even a trace amount of the element is potentially disastrous when ingested [38,39]. The United Nations Environmental Programme (UNEP) estimated that an annual release of mercury was 4400 and 7500 metric tonnes [40] as a result of natural sources and human activities, respectively [41], which contaminates the food chain and the environment. Hence, detection of mercury is very important from the environmental safety aspect.

In this paper, we report on the synthesis of tin oxide nanoparticles/graphene nanocomposite using a facile microwave method. The prepared nanocomposite was characterized using an XRD, FESEM and XPS. Electrochemical analysis was performed on the nanocomposite to investigate its ability to demonstrate determination of mercury(II) ions in potassium chloride supporting electrolyte.

2. Experimental

2.1. Materials

Graphite flakes were purchased from Ashbury Inc., sulfuric acid (H_2SO_4, 98%), potassium permanganate ($KMnO_4$, 99.9%), hydrogen peroxide (H_2O_2, 30%), hydrochloric acid (HCl, 37%) and sodium chloride (NaCl, 99.5%) were purchased from Merck. Tin(II) chloride dihydrate ($SnCl_2{\cdot}2H_2O$, 98%) and ammonia solution (NH_3, ~25%) were purchased from R&M Chemicals. Sodium hydroxide (NaOH, 99.99%), potassium chloride (KCl, 100%) and mercury(II) chloride ($HgCl_2$, 98%) were purchased from HmbG Chemicals, J.T. Baker and Fischer General Scientific, respectively. Distilled water was used throughout the sample preparation.

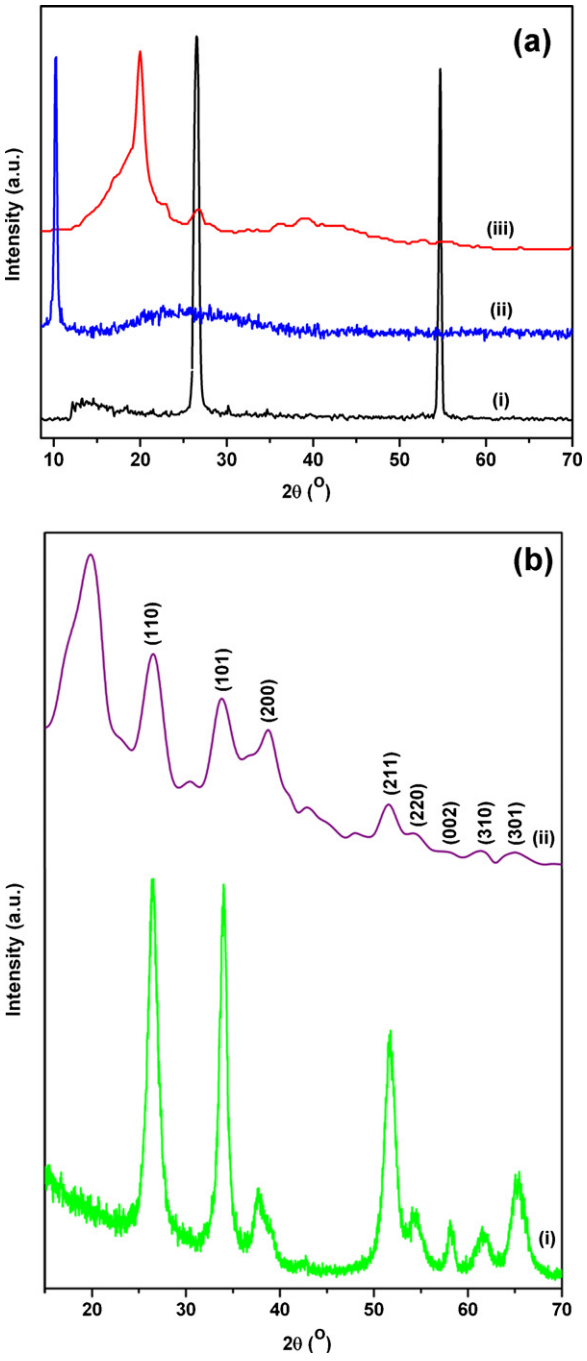

Fig. 1. XRD patterns of (a) graphite (i), GO (ii) and rGO (iii) and (b) SnO_2 nanoparticles (i) and SnO_2/GP nanocomposite (ii).

2.2. Synthesis of graphene oxide

Oxidation was carried out by mixing graphite flakes (3 g), H_2SO_4 (400 ml) and $KMnO_4$ (18 g) using a magnetic stirrer at room temperature. After that, the one pot mixture was left to stir for 3 days for a complete oxidation of graphite. The color of the mixture changed from dark purplish green to dark brown. H_2O_2 solution was added to stop the oxidation process and the color of the mixture changed to bright yellow, indicating high oxidation level of graphite oxide. The formed graphite oxide was washed with 1 M of HCl aqueous solution 3 times and deionized water repeatedly for 10 times until a pH of 4–5 was achieved. The washing process was carried out using a simple decantation of supernatant via centrifugation. During the washing process with deionized water, the graphite oxide experienced exfoliation, which resulted in the thickening of the graphene oxide (GO) solution, forming GO gel. Finally, the resulting gel was freeze-dried to obtain GO solid.

2.3. Synthesis of tin oxide nanoparticles/graphene nanocomposite via a microwave method

After the freeze-drying process, 0.4 mg/ml of the GO was mixed with 0.025 M of $SnCl_2{\cdot}2H_2O$. Then, 0.05 M of NaOH was added dropwise into the solution while stirring. The solution was transferred to a 50 ml Duran bottle and heated using a microwave oven for 20 min. The solution was allowed to cool at room temperature and the precipitate was centrifuged and washed several times with distilled water to remove the ions. Pure tin oxide powder was prepared using the same procedure.

2.4. Characterization

Crystalline phase was determined using a Phillip XRD employing a scanning rate of $0.033^\circ\ s^{-1}$ in a 2θ range from 8° to 70° with Cu Kα radiation ($\lambda = 1.5418$ Å). Electron micrographs were obtained using a FEI Nova NanoSEM 400 FESEM. Chemical composition was analyzed using a Kratos AXIS Ultra DLD XPS in a range of 0–800 eV.

2.5. Cyclic voltammetry

A Model BAS 50W electrochemical analyzer from Bioanalytical System Inc., USA was used for the cyclic voltammetry (CV) study. It was equipped with an electrochemical cell consisted of three electrodes, which were a glassy carbon electrode (GCE, 3 mm in diameter) as working electrode, a Ag/AgCl (in 3 M NaCl) as reference electrode and a platinum wire as counter electrode. Before modification, the bare GCE was polished to a mirror-like appearance with alumina slurry on micro-cloth pads, rinsed thoroughly with distilled water between each polishing step, then washed successively with distilled water and anhydrous alcohol. For

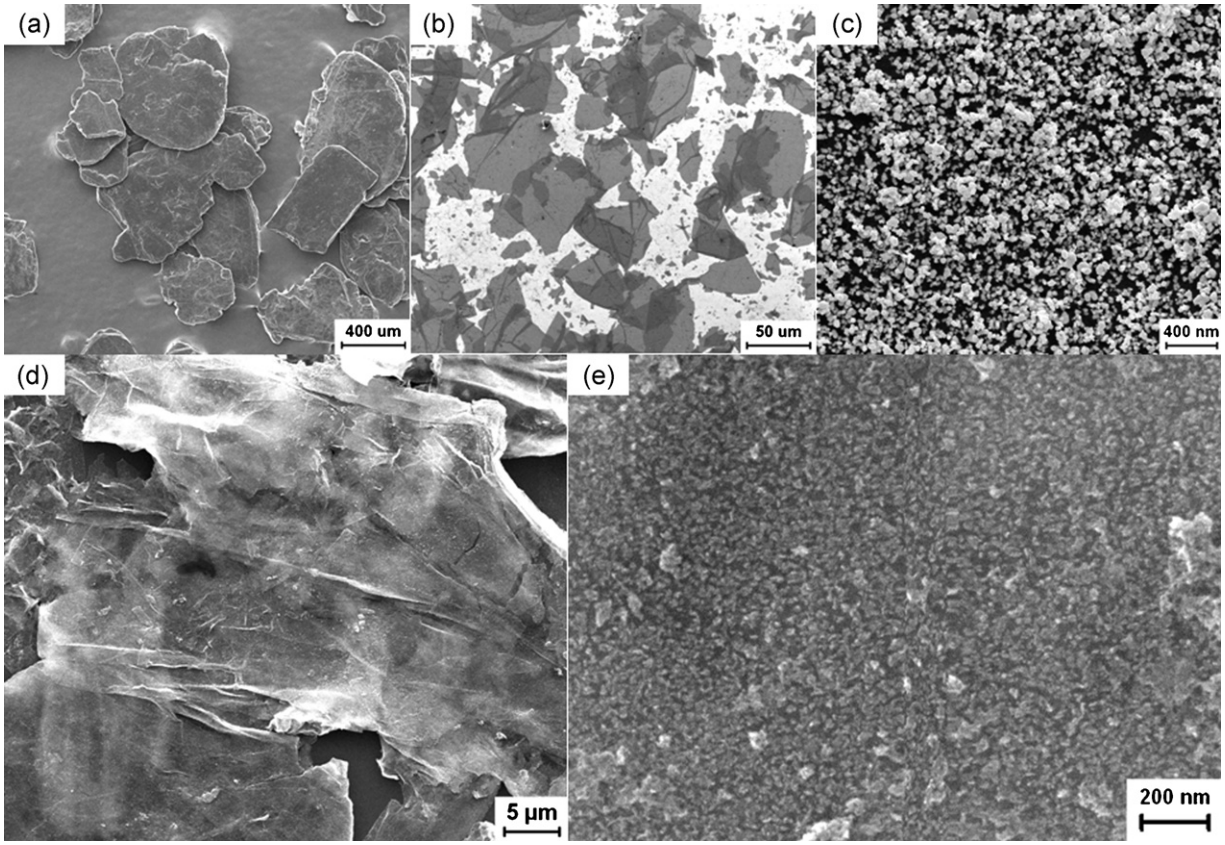

Fig. 2. FESEM images of (a) graphite flakes, (b) GO nanosheets, (c) SnO_2 nanoparticles, (d) SnO_2/GP nanocomposite at low magnification and (d) high magnification.

preparation of modified electrode, the nanocomposite was introduced onto the bare GCE by tapping the GCE successively for 10 times onto the nanocomposite [42]. 10 ml of 0.1 M of KCl as supporting electrolyte was pipetted into an electrochemical cell. 190 μl of 1.0 mM of $HgCl_2$ was used as analyte. Then, all the three electrodes were immersed into the supporting electrolyte solution. N_2 gas was bubbled into the solution for 15 min to remove the dissolved oxygen before the voltammogram was recorded. Potential range was checked before any readings on the voltammogram were recorded. All the voltammetric experiments were carried out at ambient temperature of 25 ± 2 °C.

3. Results and discussion

For the purpose of XRD analysis, GO was reduced using 2 M of NaOH. Fig. 1a shows that the diffraction peaks of pristine graphite at 26.5° (black line), GO at 9.1° (blue line) and reduced GO (rGO) at 20° (red line) corresponded to the layer-to-layer distance of 3.36 Å, 9.68 Å and 4.45 Å, respectively. The interlayer distance for GO is significantly larger than pristine graphite due to the intercalating oxide functional groups [43]. Meanwhile the interlayer distance for rGO is one-fold lower than GO, indicating the removal of the oxygenous groups on GO after the reduction by NaOH. The approximate 1 Å of difference in the interlayer distance between the pristine graphite and rGO is plausibly because it is impossible to revive the original π–π stacking between the graphene sheets after the extreme intercalation of ions into the graphite during the chemical oxidation process. The large GO sheets probably crumpled during the exfoliation stage and remained in that position after reduction during the microwave process. The reduction of GO is also confirmed by the absence of the peak at 9.1°.

Fig. 1b exhibits that the tin oxide powder corresponded to the rutile phase of SnO_2 with tetragonal structure (green line), which is indexed to JCPDS file no. 41-1445. No other peak of impurity was detected. The diffraction pattern of the nanocomposite displays that the GO was reduced to rGO after the microwave treatment (purple line). The interlayer distance of the rGO at 20° for the nanocomposite is 4.44 Å, which is almost in absolute agreement with the pure rGO, suggesting the reduction of GO at the same degree. All the other peaks are in excellent agreement with the SnO_2 structure. The broad diffraction peaks of the SnO_2 in the nanocomposite indicated small crystallite size.

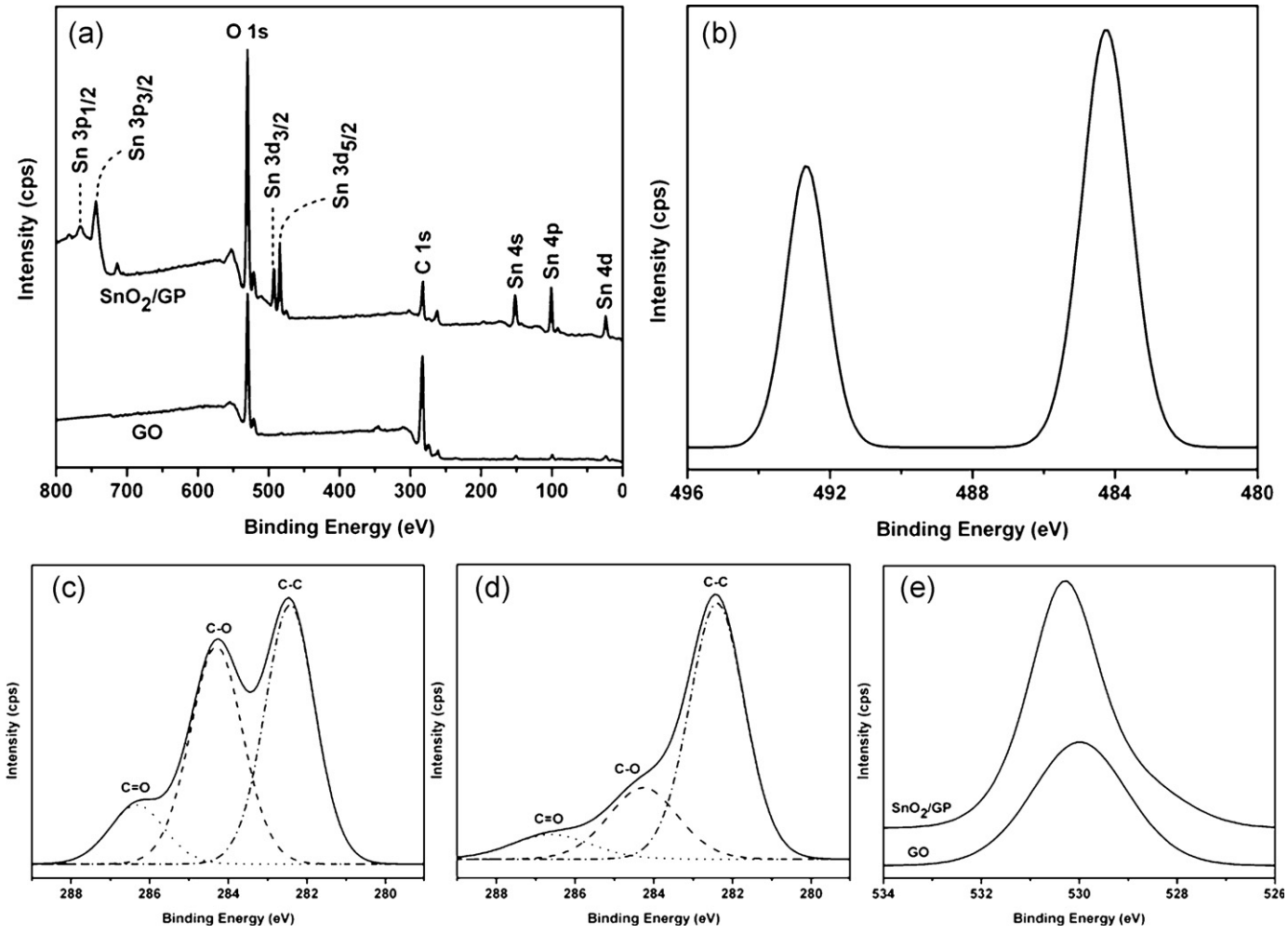

Fig. 3. XPS spectra of (a) GO and SnO_2/GP in the wide range, (b) Sn 3d doublet of SnO_2/GP, (c) C 1s of GO, (d) C 1s of SnO_2/GP and (e) O 1s of GO and SnO_2/GP.

Fig. 2a and b shows the FESEM images of the graphite flakes and the resulting GO nanosheets, respectively. The size of the GO is large with an average area of 7000 μm^2 and lateral dimension of up to 100 μm. The same GO nanosheets were used for the synthesis of SnO_2 nanoparticles/graphene (SnO_2/GP) nanocomposite. Fig. 2c shows that the SnO_2 nanoparticles prepared using the microwave method have an average diameter of 50 nm. Fig. 2d illustrates the FESEM image of SnO_2/GP, in which the graphene appeared to be wrinkly and wavy. At a higher magnification as exhibited in Fig. 2e, the SnO_2 nanoparticles are observed to adhere on the graphene sheets, in which the nanoparticles are uniformly distributed on the 2-D nanosheets with high density. The average size of the SnO_2 nanoparticles in the nanocomposite is 10 nm, which is smaller than the pure SnO_2 as the GO provided reaction sites that inhibited particle agglomeration.

In Fig. 3a, the wide XPS spectrum shows the peaks of tin (Sn 3p, 3d, 4s, 4p, 4d) for SnO_2/GP, which are attributed to SnO_2 [44]. Both GO and SnO_2/GP have C 1s and O 1s peaks. The Sn $3d_{5/2}$ and Sn $3d_{3/2}$ with respective binding energies of 484.2 eV and 492.8 eV as illustrated in Fig. 3b further confirmed the formation of SnO_2 [45]. Fig. 3c shows that the C 1s spectrum of GO was fitted with three curves at 286.5, 284.5, and 283.0 eV, fingerprints of C=O, C–O and C–C bonds, respectively [46]. The C 1s spectrum of SnO_2/GP shows a significant decrease in the C–O components relative to C–C as depicted in Fig. 3d. This suggests that the oxygen containing groups have been removed by the Sn^{2+} ions, which proves that the Sn^{2+} ions

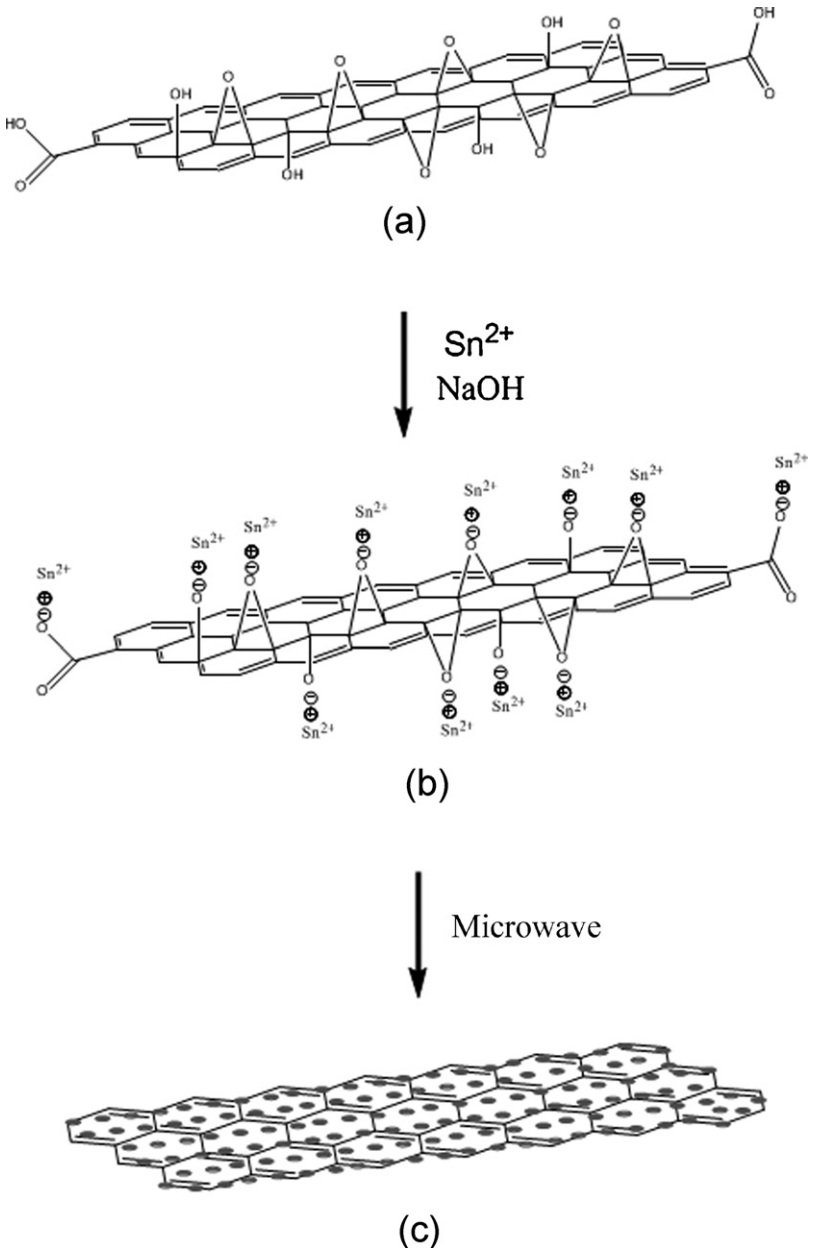

Fig. 4. Schematic formation mechanism of SnO_2/GP nanocomposite. (a) GO, (b) electrostatic interaction between oxide functional groups of GO and Sn^{2+} in the presence of NaOH and (c) graphene decorated with SnO_2 nanoparticles (filled circles) after the microwave treatment.

resulted in the deoxygenation process of GO [47]. Fig. 3e displays an obvious peak shift of approximately 0.5 eV for the O 1s spectrum of SnO_2/GP compared to that of GO, which is due to the existence of O^{2-} species in the nanocomposite [47].

A plausible schematic formation of SnO_2/GP is depicted in Fig. 4. GO is mixed with Sn^{2+} in the presence of NaOH. This provides a platform for electrostatic interaction between the negatively charged oxide functional groups of GO and positively charged Sn^{2+} as shown in Fig. 4b. Nucleation occurs at the sites, which resulted in the growth of SnO_2 nanoparticles on the 2-D graphene nanosheets during the microwave process as depicted in Fig. 4c. GO was reduced to graphene due to the simultaneous presence of Sn^{2+}, NaOH and microwave treatment.

The electrochemical performance of the SnO_2/GP, examined by cyclic voltammetry with a scan rate of 50 mV/s, is exhibited in Fig. 5. The background current behavior for bare GCE in KCl supporting electrolyte is almost plateau for oxidizing and reducing reactions (blue line) as shown in Fig. 5a. SnO_2/GP modified GCE in KCl supporting electrolyte has a similar feature (green line). In contrast, the presence of mercury(II) ions (Hg^{2+}) in KCl supporting electrolyte resulted in a distinctive oxidizing peak current, which is observed between +0.1 V and +0.2 V (I) (red line) vs Ag/AgCl. SnO_2/GP modified GCE in KCl supporting electrolyte spiked with Hg^{2+} resulted in the appearance of double oxidative peaks and enhanced the reductive current by more than ten fold, in addition to the appearance of two reductive peaks between −0.1 and +0.1 V (II) and +0.3 and +0.7 (III) (purple line). All the peaks are most likely to arise through the stepwise reduction of $Hg^{2+} + e^- \rightleftarrows Hg^+$ and $Hg^+ + e^- \rightleftarrows Hg^0$.

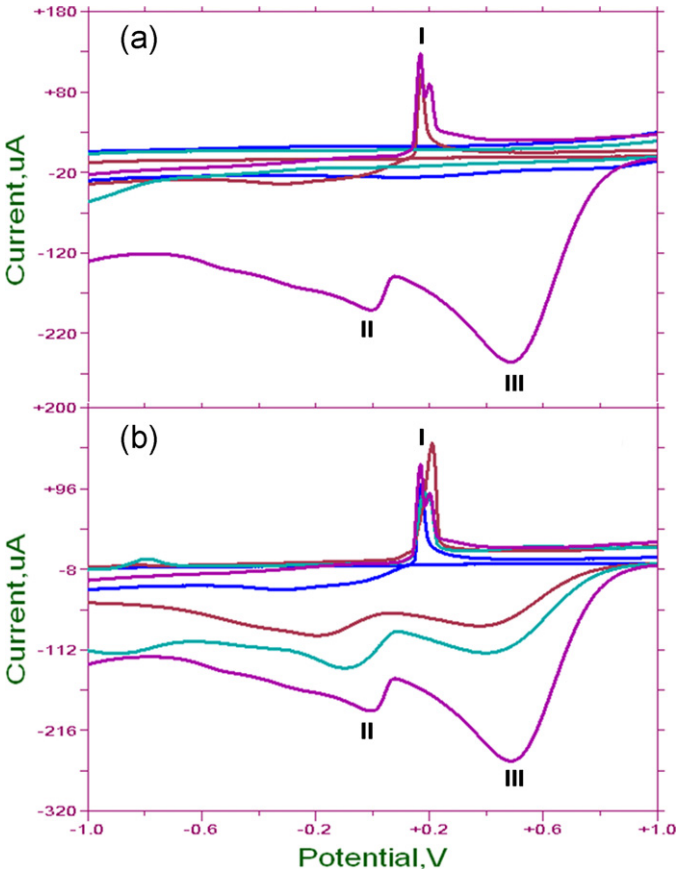

Fig. 5. (a) Electrochemical analysis of (a) bare GCE in KCl supporting electrolyte (blue line), bare GCE in KCl supporting electrolyte and Hg^{2+} ionic solution (red line), SnO_2/GP modified GCE in KCl supporting electrolyte (green line) and SnO_2/GP modified GCE in KCl supporting electrolyte and Hg^{2+} ionic solution (purple line), and (b) bare (blue line), GO (red line), SnO_2 nanoparticles (green line) and SnO_2/GP (purple line) modified GCE in KCl supporting electrolyte and Hg^{2+} ionic solution. (For interpretation of the references to color in this figure legend, the reader is referred to the web version of the article.)

The comparison for the electrochemical performance of GO, SnO_2 nanoparticles and SnO_2/GP is depicted in Fig. 5b. Bare GCE in KCl supporting electrolyte and Hg^{2+} ionic solution is shown by the blue line. GO modified GCE (red line) exhibits similar oxidative and reductive peaks as SnO_2/GP (purple line). However, the reductive current was reduced tremendously by more than 100 μA even though there is a slight increase in the oxidative current. A plausible explanation could be that the oxygenous groups of GO such as hydroxyl, epoxy and carboxyl [48] on the basal and edges of the 2-D nanosheets hinder the mobility of electrons, which fundamentally decrease the conductivity of the 2-D carbon lattice [49]. There is an improvement in the reductive current for SnO_2 nanoparticles compared to GO by approximately 40 μA (green line). The combination of the two components yielded the best electrochemical performance as there is a significant increase, particularly, in the reductive current, signifying increased sensitivity to the detection of Hg^{2+}. The excellent electrochemical activity is contributed by the fact that the hybridization of both the materials led to a highly conductive medium for fast electron transfer during the redox reaction. The redox process of Hg(II) was contributed by every sample present on the GC electrode surface. Among all the samples, SnO_2/GP possessed the best reducing reaction, which possibly makes it an efficient redox-recyclable material for the extraction of heavy element ions from waste water [50].

4. Conclusion

We had successfully synthesized a hybrid of SnO_2 nanoparticles decorated on graphene nanosheets. The prepared nanocomposite exhibited excellent electrochemical performance by increasing the reductive current by more than 10 times. The highly enhanced reductive peak current compared to the oxidative peak current indicates that mercury(II) ions could easily be reduced to mercury metal, suggesting that the nanocomposite modified GCE may be a potential tool for detection and removal of the hazardous metal. Further experimentations are necessary to analyze the ability of the nanocomposite to detect and absorb mercury metal, in the hope that it possesses bi-functional properties as a chemical sensor as well as an absorber.

Acknowledgements

This work was supported by the University of Malaya Research Grant (RG197/11AFR), the High Impact Research

Grant of the University of Malaya (UM.C/625/1/HIR/030) and the High Impact Research Grant from the Ministry of Higher Education (UM.C/625/1/HIR/MOHE/05). We thank Mr. Mohamad Azri Tukimon for help with the XPS characterization.

References

[1] N.M. Huang, S. Radiman, H.N. Lim, S.K. Yeong, P.S. Khiew, W.S. Chiu, G.H.M. Saeed, K. Nadarajah, Gamma-ray assisted synthesis of Ni_3Se_2 nanoparticles stabilized by natural polymer, Chemical Engineering Journal 147 (2009) 399–404.

[2] N.M. Huang, S. Radiman, H.N. Lim, S.K. Yeong, P.S. Khiew, W.S. Chiu, S.N. Kong, G.H. Mohamed Saeed, Synthesis and characterization of ultra small PbS nanorods in sucrose ester microemulsion, Materials Letters 63 (2009) 500–503.

[3] W.S. Chiu, P.S. Khiew, D. Isa, M. Cloke, S. Radiman, R. Abd-Shukor, M.H. Abdullah, N.M. Huang, Synthesis of two-dimensional ZnO nanopellets by pyrolysis of zinc oleate, Chemical Engineering Journal 142 (2008) 337–343.

[4] W.S. Chiu, P.S. Khiew, M. Cloke, D. Isa, H.N. Lim, T.K. Tan, N.M. Huang, S. Radiman, R. Abd-Shukor, M.A.A. Hamid, C.H. Chia, Heterogeneous seeded growth: synthesis and characterization of bifunctional Fe_3O_4/ZnO core/shell nanocrystals, The Journal of Physical Chemistry C 114 (2010) 8212–8218.

[5] R. Liang, M. Deng, S. Cui, H. Chen, J. Qiu, Direct electrochemistry and electrocatalysis of myoglobin immobilized on zirconia/multi-walled carbon nanotube nanocomposite, Materials Research Bulletin 45 (2010) 1855–1860.

[6] Z. Li, W. Shen, X. Zhang, L. Fang, X. Zu, Controllable growth of SnO_2 nanoparticles by citric acid assisted hydrothermal process, Colloids and Surfaces A: Physicochemical Engineering Aspects 327 (2008) 17–20.

[7] S. Das, S. Chaudhuri, S. Maji, Ethanol–water mediated solvothermal synthesis of cube and pyramid shaped nanostructured tin oxide, The Journal of Physical Chemistry C 112 (2008) 6213–6219.

[8] J. Ning, Q. Dai, T. Jiang, K. Men, D. Liu, N. Xiao, C. Li, D. Li, B. Liu, B. Zou, G. Zou, W.W. Yu, Facile synthesis of tin oxide nanoflowers: a potential high-capacity lithium-ion-storage material, Langmuir 25 (2008) 1818–1821.

[9] H. Wang, F. Sun, Y. Zhang, L. Li, H. Chen, Q. Wu, J.C. Yu, Photochemical growth of nanoporous SnO_2 at the air–water interface and its high photocatalytic activity, Journal of Materials Chemistry (2010) 5641–5645.

[10] B.M. Matin, Y. Mortazavi, A.A. Khodadadi, A. Abbasi, A.A. Firooz, Alkaline- and template-free hydrothermal synthesis of stable SnO_2 nanoparticles and nanorods for CO and ethanol gas sensing, Sensors and Actuators B 151 (2010) 140–145.

[11] K.S. Novoselov, A.K. Geim, S.V. Morozov, D. Jiang, Y. Zhang, S.V. Dubonos, I.V. Grigorieva, A.A. Firsov, Electric field effect in atomically thin carbon films, Science 306 (2004) 666–669.

[12] R.R. Nair, P. Blake, A.N. Grigorenko, K.S. Novoselov, T.J. Booth, T. Stauber, N.M.R. Peres, A.K. Geim, Fine structure constant defines visual transparency of graphene, Science 320 (2008) 1308.

[13] J.S. Bunch, A.M. van der Zande, S.S. Verbridge, I.W. Frank, D.M. Tanenbaum, J.M. Parpia, H.G. Craighead, P.L. McEuen, Electromechanical resonators from graphene sheets, Science 315 (2007) 490–493.

[14] A. Yu, P. Ramesh, M.E. Itkis, E. Bekyarova, R.C. Haddon, Graphite nanoplatelet-epoxy composite thermal interface materials, The Journal of Physical Chemistry C 111 (2007) 7565–7569.

[15] M.D. Stoller, S. Park, Y. Zhu, J. An, R.S. Ruoff, Graphene-based ultracapacitors, Nano Letters 8 (2008) 3498–3502.

[16] F. Chen, N.J. Tao, Electron transport in single molecules: from benzene to graphene, Accounts of Chemical Research 42 (2009) 429–438.

[17] M. Pumera, The electrochemistry of carbon nanotubes: fundamentals and applications, Chemistry-A European Journal 15 (2009) 4970–4978.

[18] M. Pumera, Electrochemistry of graphene: new horizons for sensing and energy storage, The Chemical Record 9 (2009) 211–223.

[19] M. Pumera, Imaging of oxygen-containing groups on walls of carbon nanotubes, Chemistry-An Asian Journal 4 (2009) 250–253.

[20] X. Zhou, X. Huang, X. Qi, S. Wu, C. Xue, F.Y.C. Boey, Q. Yan, P. Chen, H. Zhang, In situ synthesis of metal nanoparticles on single-layer graphene oxide and reduced graphene oxide surfaces, The Journal of Physical Chemistry C 113 (2009) 10842–10846.

[21] A.P. Alivisatos, Semiconductor clusters, nanocrystals, and quantum dots, Science 271 (1996) 933–937.

[22] H. Fissan, M.K. Kennedy, T.J. Krinke, F.E. Kruis, Nanoparticles from the gas phase as building blocks for electrical devices, Journal of Nanoparticle Research 5 (2003) 299–310.

[23] A.K. Geim, Graphene: status and prospects, Science 324 (2009) 1530–1534.

[24] A.K. Geim, K.S. Novoselov, The rise of graphene, Nature Materials 6 (2007) 183–191.

[25] G. Lu, S. Mao, S. Park, R. Ruoff, J. Chen, Facile, noncovalent decoration of graphene oxide sheets with nanocrystals, Nano Research 2 (2009) 192–200.

[26] S. Chen, J. Zhu, X. Wang, An in situ oxidation route to fabricate graphene nanoplate-metal oxide composites, Journal of Solid State Chemistry 184 (2011) 1393–1399.

[27] Y.J. Mai, X.L. Wang, J.Y. Xiang, Y.Q. Qiao, D. Zhang, C.D. Gu, J.P. Tu, CuO/graphene composite as anode materials for lithium-ion batteries, Electrochimica Acta 56 (2011) 2306–2311.

[28] S. Moussa, V. Abdelsayed, M.S. El-Shall, Laser synthesis of Pt, Pd, CoO and Pd–CoO nanoparticle catalysts supported on graphene, Chemical Physics Letters 510 (2011) 179–184.

[29] G. Wang, T. Liu, Y. Luo, Y. Zhao, Z. Ren, J. Bai, H. Wang, Preparation of Fe_2O_3/graphene composite and its electrochemical performance as an anode material for lithium ion batteries, Journal of Alloys and Compounds 509 (2011) L216–L220.

[30] P. Lian, X. Zhu, H. Xiang, Z. Li, W. Yang, H. Wang, Enhanced cycling performance of Fe_3O_4-graphene nanocomposite as an anode material for lithium-ion batteries, Electrochimica Acta 56 (2010) 834–840.

[31] B. Wang, J. Park, C. Wang, H. Ahn, G. Wang, Mn_3O_4 nanoparticles embedded into graphene nanosheets: preparation, characterization, and electrochemical properties for supercapacitors, Electrochimica Acta 55 (2011) 6812–6817.

[32] I.R.M. Kottegoda, N.H. Idris, L. Lu, J.-Z. Wang, H.-K. Liu, Synthesis and characterization of graphene-nickel oxide nanostructures for fast charge–discharge application, Electrochimica Acta 56 (2011) 5815–5822.

[33] P. Lian, X. Zhu, S. Liang, Z. Li, W. Yang, H. Wang, High reversible capacity of SnO_2/graphene nanocomposite as an anode material for lithium-ion batteries, Electrochimica Acta 56 (2011) 4532–4539.

[34] S. Wang, S.P. Jiang, X. Wang, Microwave-assisted one-pot synthesis of metal/metal oxide nanoparticles on graphene and their electrochemical applications, Electrochimica Acta 56 (2011) 3338–3344.

[35] J. Yao, X. Shen, B. Wang, H. Liu, G. Wang, In situ chemical synthesis of SnO_2-graphene nanocomposite as anode materials for lithium-ion batteries, Electrochemistry Communications 11 (2009) 1849–1852.

[36] J. Guo, S. Zhu, Z. Chen, Y. Li, Z. Yu, Q. Liu, J. Li, C. Feng, D. Zhang, Sonochemical synthesis of TiO_2 nanoparticles on graphene for use as photocatalyst, Ultrasonics Sonochemistry 18 (2011) 1082–1090.

[37] H. Zhang, X. Lv, Y. Li, Y. Wang, J. Li, P25-graphene composite as a high performance photocatalyst, ACS Nano 4 (2010) 380–386.

[38] Y.M. Panta, J. Liu, M.A. Cheney, S.W. Joo, S. Qian, Ultrasensitive detection of mercury(II) ions using electrochemical surface plasmon resonance with magnetohydrodynamic convection, Journal of Colloid and Interface Science 333 (2009) 485–490.

[39] M. Yamamoto, T. Charoenraks, H. Pan-Hou, A. Nakano, A. Apilux, M. Tabata, Electrochemical behaviors of sulfhydryl compounds in the presence of elemental mercury, Chemosphere 69 (2007) 534–539.

[40] J. Liu, Y. Lu, Rational design of turn-on allosteric DNAzyme catalytic beacons for aqueous mercury ions with ultrahigh sensitivity and selectivity, Angewandte Chemie International Edition 46 (2007) 7587–7590.

[41] H. Li, J. Zhai, J. Tian, Y. Luo, X. Sun, Carbon Nanoparticle for Highly Sensitive and Selective Fluorescent Detection of Mercury(II) Ion in Aqueous Solution, Biosensors and Bioelectronics, 2011.

[42] A.M. Bond, F. Marken, Mechanistic aspects of the electron and ion transport processes across the electrode solid solvent (electrolyte) interface of microcrystalline decamethylferrocene attached mechanically to a graphite electrode, Journal of Electroanalytical Chemistry 372 (1994) 125–135.
[43] A. Lerf, A. Buchsteiner, J. Pieper, S. Schöttl, I. Dekany, T. Szabo, H.P. Boehm, Hydration behavior and dynamics of water molecules in graphite oxide, Journal of Physics and Chemistry of Solids 67 (2006) 1106–1110.
[44] F. Li, J. Song, H. Yang, S. Gan, Q. Zhang, D. Han, A. Ivaska, L. Niu, One-step synthesis of graphene/SnO_2 nanocomposites and its application in electrochemical supercapacitors, Nanotechnology 20 (2009) 455602–455608.
[45] Q. Zhao, Z. Zhang, T. Dong, Y. Xie, Facile synthesis and catalytic property of porous tin dioxide nanostructures, The Journal of Physical Chemistry B 110 (2006) 15152–15156.
[46] K.-H. Liao, Y.-S. Lin, C.W. Macosko, C.L. Haynes, Cytotoxicity of graphene oxide and graphene in human erythrocytes and skin fibroblasts, ACS Applied Materials & Interfaces (2011) 2607–2615.
[47] Y. Li, X. Lv, J. Lu, J. Li, Preparation of SnO_2-nanocrystal/graphene-nanosheets composites and their lithium storage ability, The Journal of Physical Chemistry C 114 (2010) 21770–21774.
[48] X. Zhao, Q. Zhang, Y. Hao, Y. Li, Y. Fang, D. Chen, Alternate multilayer films of poly(vinyl alcohol) and exfoliated graphene oxide fabricated via a facial layer-by-layer assembly, Macromolecules 43 (2010) 9411–9416.
[49] S.Z. Zu, B.H. Han, Aqueous dispersion of graphene sheets stabilized by pluronic copolymers: formation of supramolecular hydrogel, Journal of Physical Chemistry C 113 (2009) 13651–13657.
[50] P.K. Dorhout, S.H. Strauss, The design, synthesis, and characterization of redox-recyclable materials for efficient extraction of heavy element ions from aqueous waste streams, Inorganic Materials Synthesis 727 (1999) 53–68.